Physica E 148 (2023) 115655

Contents lists available at ScienceDirect

Physica E: Low-dimensional Systems and Nanostructures

journal homepage: www.elsevier.com/locate/physe

Edge reconstruction of 2D-Xene (X = Si, Ge, Sn) zigzag nanoribbons

Yuqiang Gao [a,*], Geert Brocks [b]

[a] Department of Physics, School of Physics and Electronic Information, Anhui Normal University, Wuhu, 241000, PR China
[b] Faculty of Science and Technology and MESA+ Institute for Nanotechnology, University of Twente, Enschede, 7500AE, The Netherlands

ARTICLE INFO

Keywords:
2D-Xene
Zigzag edge reconstruction
First principle calculations
Tight binding model

ABSTRACT

By performing first principles calculations, we investigate the edge reconstruction in free-standing 2D-Xene (X = Si, Ge, Sn) zigzag nanoribbons. Three different periodicities of edge reconstruction ($2a, 3a, 4a$) are found, in which the reconstruction with $3a$ periodicity has the lowest energy and shows non-magnetic ground state. The edge reconstruction can be understood by the reconfiguration of the dangling bond states and edge states at the zigzag edges. Due to the structural buckling, extra bonding states are formed between edge atoms and inner atoms, accompanied with charge transfer from the edge states to the dangling bond states. This results in one-third occupied dangling bond states and a Peierls-like structural reconstruction with $3a$ periodicity at the edge which opens a small band gap. With a tight binding model, the reconstruction of the electronic structures at the edges are revealed by the hopping integrals between different edge X-p orbitals.

1. Introduction

In wake of graphene, the single-element, monoatomic honeycomb lattices of two-dimensional (2D) Xene, where X = Si, Ge, or Sn (silicene, germanene, stanene), have attracted great attention for their rich and exotic electronic properties [1–5]. In contrast to the flat honeycomb lattice of graphene, the honeycomb lattice of silicene, germanene and stanene have a buckling between the A and B sublattices [6], breaking the mirror symmetry along the plane and decreasing the local lattice symmetry from D_{6h} to D_{3d}. The lowering symmetry and larger atomic number of silicon, germanium, and tin as compared to carbon induce a much stronger spin orbit coupling (SOC) in 2D-Xene [7,8], which generates novel electronic states, such as topological protected gapless helical modes at the edges and a quantum spin Hall effect [5].

Whereas these 2D layers may be interesting for applications in electronics, scientific interest has also focused on the electronic properties of the 2D-Xene nanoribbons, which are one-dimensional (1D) stripes "cut" from the corresponding 2D-Xene monolayers. The nanoribbons are typical several nanometers in width and quasi-infinite in length. The most prominently different edge orientations of honeycomb lattices are called armchair and zigzag edges respectively, see Fig. 1. The edges of 2D nanosheets introduce edge states and affect the properties of the nanosheets [9]. The armchair edge is typically insulating, and thus mostly harmless. The zigzag edge is more interesting, as in its pristine form it is metallic, and as such, it is prone to electronic and structural instabilities [10].

The edge states are best understood for graphene [11,12], where the carbon atoms are in-plane σ-bonded by sp^2 orbitals, and π-bonded by out-of-plane p_z orbitals. For each carbon atom at the zigzag edge, one σ-bond is missing, leading to an in-plane sp^2 dangling bond state. In addition, each such edge carbon atom carries an edge states formed by the π–p_z state. In buckled X-ene nanoribbons, the two states at a zigzag edge discussed above, are still present, but they can now hybridize because of the broken symmetry. This is consistent with the bonding between the atoms being closer to sp^3 σ-bonds, which promotes a non-planar structure. The edge states and reconstructions of Xene edges are therefore potentially more diverse than those of graphene. Such as various edge reconstructions were reported for silicene zigzag nanoribbons [13–16], which are sensitive to the width and strain.

The edge states can be stabilized by edge reconstruction [17,18], edge passivation [19], and edge closure [20]. Dangling bond states and edge states in graphene zigzag nanoribbons each give a relatively flat edge band containing unpaired electrons, which yields a high density of states (DOS) near the Fermi level. Such a 1D metallic structure is susceptible to structural instabilities. For instance, an edge reconstruction that includes Stone–Wales defects or Klein edges [12,17,18], lifts the dangling bond state away from the Fermi level [21]. Alternatively, if the zigzag edge is passivated by hydrogen atoms, the dangling bond state can be removed completely. This still leaves the p_z edge band giving a non-trivial (magnetic) electronic structure, however [22,23]. Edge closure is observed in multilayered graphene, where the zigzag edges between adjacent graphene layers are closed after thermal treatment [20]. The itinerant magnetism introduced by the high DOS near the Fermi level is believed to be too weak to compete with the structural reconstruction [11]. Computationally, X-ene zigzag edges have

* Corresponding author.
E-mail addresses: y.gao@ahnu.edu.cn (Y. Gao), g.h.l.a.brocks@utwente.nl (G. Brocks).

https://doi.org/10.1016/j.physe.2023.115655
Received 18 October 2022; Received in revised form 9 January 2023; Accepted 10 January 2023
Available online 14 January 2023

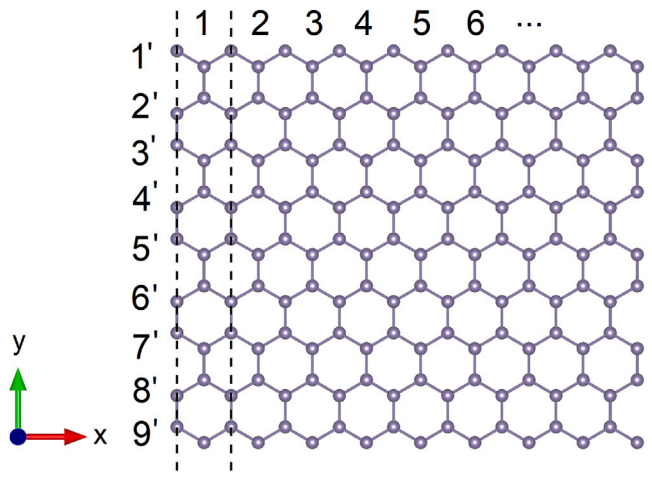

Fig. 1. Geometric structures of Germanene nanoribbons. Zigzag edges and armchair edges are along x and y direction, respectively. The dashed rectangle represents 9×1 unit cell with zigzag edges repeated in x direction.

been studied with hydrogen passivation of the edge atoms, leaving edge states that might be topological because of the significant spin–orbit coupling in these materials [15,24–27]. Such edges are treated as being unreconstructed [13]. Pristine, reconstructed silicene and germanene zigzag edges with $2a$ periodicity have also been considered [13–16], where it is believed that these are metallic and show anti-ferromagnetic ground states. Recently, Zhang et al. [1] have studied a germanene layer on top of a Ge_2Pt substrate by scanning tunnelling microscopy and spectroscopy (STM and STS) and have identified reconstructed zigzag edges with a $4a$ periodicity. The differential conductivity at the edges has a parabolic shape, and indicates that there are no pronounced metallic edge states.

Although lots of work have been done on the edge states and edge reconstruction of 2D Xene, inconsistencies exist and little has been done to systematically map out the edge states of buckled 2D X-ene nanoribbons, which are dominated by a mixed sp^2 and sp^3 hybridization. To clarify these inconsistencies and have a clear picture on the edge states of 2D Xene nanoribbons, we systematically investigate the zigzag edge reconstruction of pristine silicene, germanene and stanene nanoribbons. Surprisingly, we find that all these edges reconstruct with a $3a$ periodicity. The $3a$ periodicity can in fact be predicted from the band filling of the edge states associated with the buckled pristine edge. The reconstruction opens a gap and leads to non-magnetic ground states. The change in electronic structure can be analysed in detail with the help of a tight-binding model.

2. Computational method

We performed first principles calculations with density functional theory (DFT) using the all-electron projector augmented wave (PAW) method [28] and a plane-wave basis set with a cut-off energy of 400 eV as implemented in VASP package [29–31]. The equilibrium structural and electronic properties for silicene, germanene, and stanene were calculated in the generalized gradient approximation (GGA) [32] as listed in Table 1, which agree well with previous work [33]. Zigzag nanoribbons were periodically repeated in the x direction with 9 ribbon chains in y direction to avoid edge interaction and separated by more than 20 Å of vacuum in y and z direction to avoid spurious interaction. We fix the width of nanoribbons to 9 and construct different size of supercells labelled as $9 \times n$ (n = 1, 2, 3, 4, 5, 6, 7, 8, 9) as shown in Fig. 1. For the nanoribbons, 3 ribbon chains in the middle are fixed to mimic the corresponding bulk material and the rest atomic structures are fully relaxed until the force less than 0.001 eV/Å. $45 \times 1 \times 1$ k-point sampling is used.

Table 1
Calculated structural parameters for 2D-Xene. a, d_{X-X}, and δ represent the lattice constant, bond length, and buckling, respectively.

Xene	a (Å)	d_{X-X} (Å)	δ (Å)
Silicene	3.86	2.27	0.45
Germanene	4.05	2.44	0.69
Stanene	4.67	2.89	0.85

3. Electronic properties

The band structures and density of states (DOS) of 9×1 zigzag Germanene ribbon are plotted in Fig. 2. In Fig. 2(a), two bands introduced by the two edges are formed in the bandgap, leaving a DOS peak at the Fermi level. In flat graphene, when 2D nanosheets are cut into 1D ribbons, one missing bond at the zigzag edge atoms gives rise to edge states formed by π–p_z state and also dangling bond states formed by σ–sp^2 state in the bandgap because of one bond missing for the edge atoms. However, the buckling of the atomic lattice as in 2D Xene (X = Si, Ge, or Sn) leads to hybridization between the edge states and the dangling bond states and band dispersion as shown in Fig. 2(a). The orbital resolved DOS on edge atoms shows that the dangling bond states near the Fermi level mainly consist of p_y orbitals, while the edge states formed by p_z orbitals are pushed up at 0.5 eV. As a result, the electrons on the edge states are transferred to the dangling states.

The electronic instability induced by the DOS peak at the Fermi level leads to spin polarized edges. The edges atoms on the same side are coupled ferromagnetic. The edges atoms on the two sides are coupled antiferromagnetically (AFM) (Fig. 2(b)) but only 0.6 meV per atom lower than the ferromagnetic (FM) state (Fig. 2(c)) and 2.8 meV per atom lower than the non-magnetic (NM) state. The small difference in energy for AFM and FM states indicates the large ribbon width is sufficient to decouple the two edges.

The band structures for nonmagnetic states, in-plane antiparallel (AFM) and parallel (FM) spins with SOC are shown in Fig. 2(d), (e) and (f), respectively. As the spin orbit coupling is included, the degenerate part of edge bands near the Fermi levels split (Fig. 2(d)), which can be attributed to the symmetry breaking at the edges. The SOC lowers the total energy by 7 meV per atom with respect to the NM states. The magnetic anisotropy energy calculated for the spin polarized edges is about 0.7 meV per edge atom, where the spin prefer the in-plane direction. This is consistent with previous work [34]. The band structures of AFM states are not changed much by the SOC. In FM states, the spin up and down channels (red and black lines in Fig. 2(c)) cross at K point near the Fermi level. As shown in Fig. 2(f), the SOC open up a small band gap of 36 meV at the crossing point of spin up and down bands. This value is higher than the one found in 2D germanene (~ 23.9 meV) [5], which can be attributed to the symmetry breaking at the edges. By comparing the total energy of different states with and without SOC, the spin prefer to lie in-plane and antiparallely between two edges with about 0.6 meV per atom lower than the ferromagnetic coupling. In the following sections, the SOC effect are included for the total energy calculations. In addition, the AFM states are also considered for the spin polarized systems.

To have a better understanding of the states introduced by the edges, we compensate the dangling bond on one side of the nanoribbon (bottom edge atoms in Fig. 3(a)) by hydrogen atoms. For clarity, the SOC and spin polarization are not included. From the projected band structure Fig. 3(b–d), the dangling bond states of unpassivated edge atoms (Si, Ge, Sn) with p_y orbital character (X: p_y, X = Si, Ge, Sn) lie from Γ to K near the Fermi level and pull up the edge states (K–X) with p_z orbital character (X: p_z) by 0.5 eV, while the dangling states of the passivated edge atoms (X_H) are passivated by hydrogen and only the flat edge states with p_z orbital character (X_H: p_z) lying from K to X are left near the Fermi level. The dangling bond bands are nearly half occupied. If we further remove the edges states of the bottom edge

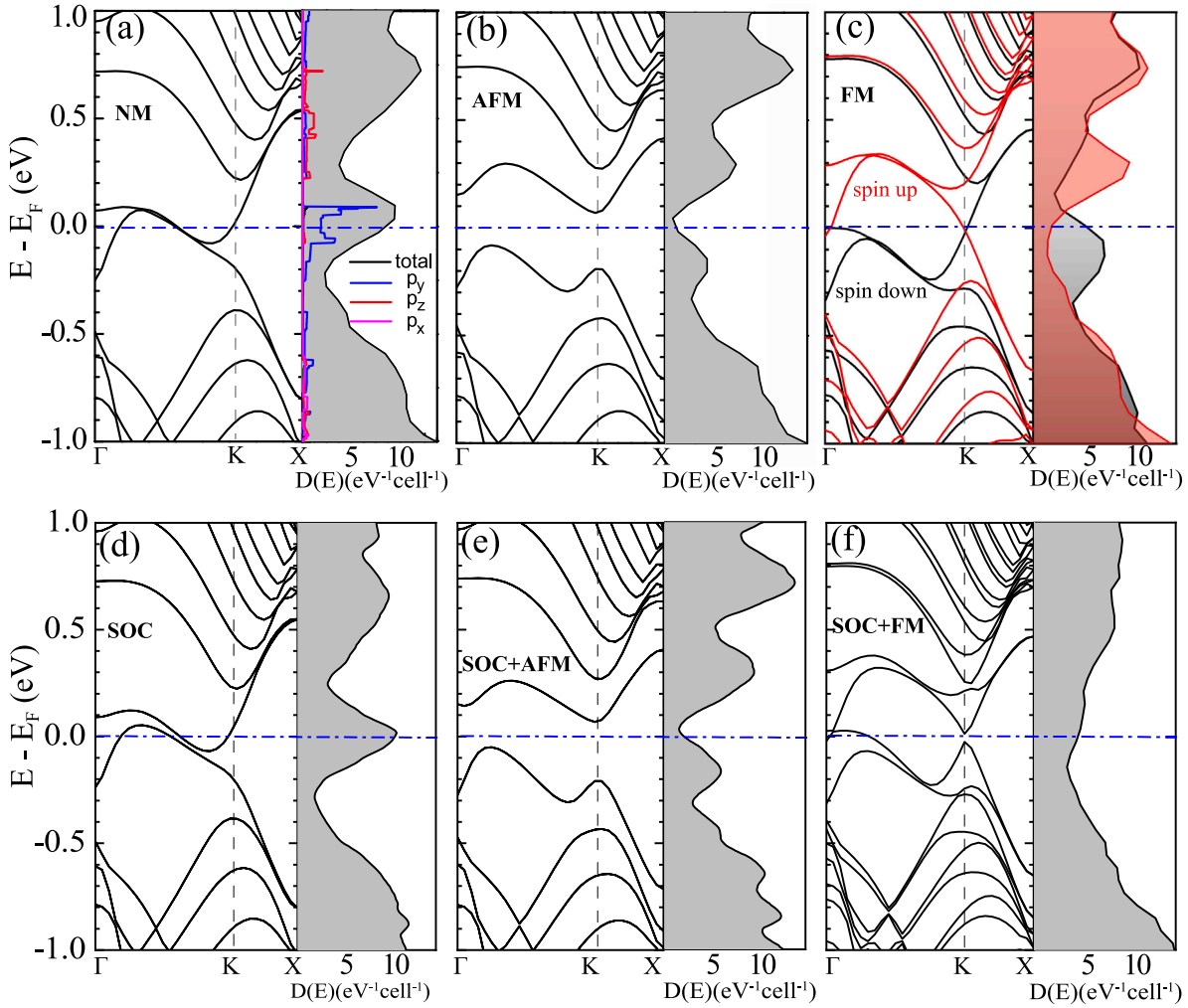

Fig. 2. Band structures and density of states of 9 × 1 zigzag Germanene ribbon with non-spin polarization (a), anti-ferromagnetic polarization (b), ferromagnetic polarization (c), spin orbit coupling (d), anti-ferromagnetic polarization with spin orbit coupling (e), and ferromagnetic polarization with spin orbit coupling (f). The projected DOS on edge atoms is shown in (a). K point denotes $\frac{1}{3}\pi$.

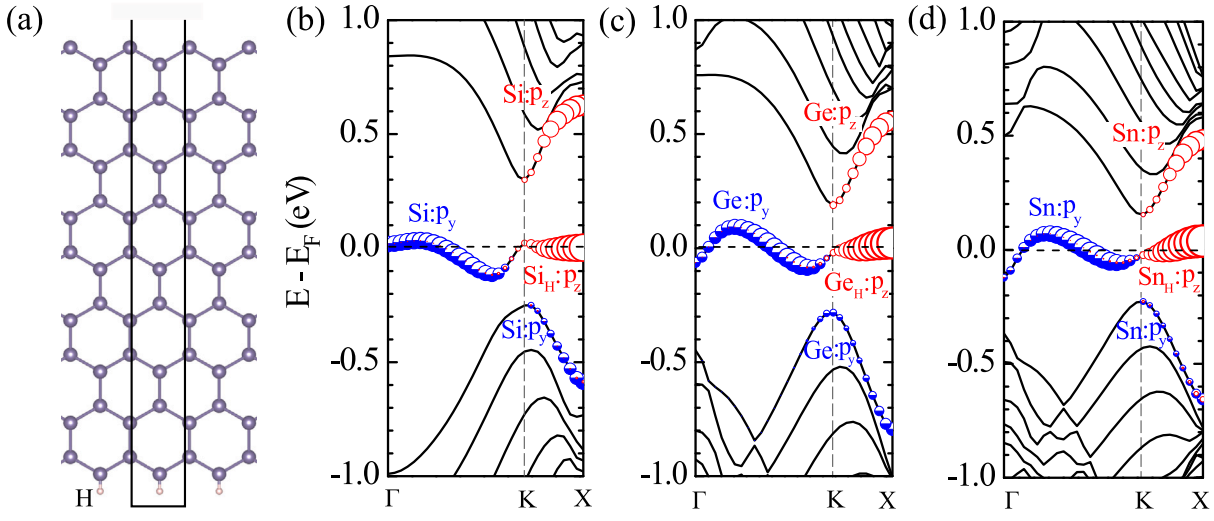

Fig. 3. Projected band structures (without SOC and spin polarization) of 9 × 1 zigzag silicene (b), germanene (c), and stanene (c) ribbons with hydrogen passivation on one side of edge atoms. The contribution from the edge atoms p_z and p_y orbitals are show as open red circles and half-filled blue circles, respectively in (b–d) where the symbol size is proportional to the population of the corresponding state. Si_H, Ge_H and Sn_H indicate edge atoms passivated by hydrogen atoms.

Table 2
Edge energies (eV/unit cell) for relaxed silicene, germanene, and stanene zigzag ribbons with different periodicity. The unit cell refers to 9 × 1 cell. The SOC are included. The AFM states are considered in E_{edge}(Silicene-2a).

n	2	3	4
E_{edge}(Silicene)	−0.38	−0.44	−0.37
E_{edge}(Germanene)	−0.43	−0.51	−0.43
E_{edge}(Stanene)	−0.22	−0.35	−0.23

atom (red circles near the Fermi level in Fig. 3(b–d)), we can see that 2/3 electron in the dangling states are unpaired, which indicates a 3a periodicity of structural reconstruction. Dangling bond states should have one unpaired electron per edge atom, while the edge states have 1/3 electron unpaired per edge atom. However, as shown in Fig. 3(b–d), only 2/3 electron from the dangling states of the edge atom appear near the Fermi level (nonbonding states). 1/3 electron from dangling states and 1/3 electron from edge states are missing. From the projected band structures, we can see that from K–X there have bonding states with p_y orbital characters (X: p_y) located just below the Fermi level. 1/3 electrons from the edge states (p_z) and 1/3 dangling states (p_y) form extra bonding states with inner atoms by a charge transfer from edge states (p_z) to dangling bond states (p_y). This extra bonding states should be related to the buckling of the structure and would be discussed in Section 6. It should be noted that the band dispersion of the dangling bond states and edge states near the Fermi level are slightly different for those three 2D-Xene nanoribbons, which would be discussed in Section 6.

4. Edge reconstruction

The electronic instability at the zigzag of 2D-Xene not only lead to breaking of the time reversal symmetry but also the spatial symmetry, namely, the edge reconstruction. We relaxed the structures of 2D-Xene nanoribbons with different supercell size 9 × n (n = 2, 3, 4, 5, 6, 7, 8, 9). The structure reconstruction greatly decreases the total energy. The energy gain from the structure reconstruction are much larger than the energy gain from the spin polarization and spin orbit coupling in Fig. 2. The effect of spin orbit coupling on the structural relaxation has been examined by comparing the forces on atoms in calculations with and without SOC for unrelaxed and relaxed structures. The force differences on each atom are on the order of 0.0001 eV/Å, which are smaller than the converge criteria of forces in the relaxations. Therefore, the SOC is not included in the structural relaxations. The structures are fully relaxed with AFM states to find the most stable structures. The relaxation generates three different kinds of periodicity: 2a, 3a and 4a. Relaxation of large supercells generate a combination of these three periodicities. For example, 9 × 7 supercell gives rise to a relaxed structure with 3a+4a periodicity. 9 × 6 supercell has the same 3a periodicity as the 9 × 3 supercell. Therefore, here we only consider the structure relaxation with these three different periodicities. We define the edge energy as

$$E_{edge} = (E_{relaxed} - E_{unrelaxed})/n \tag{1}$$

in which E_{relaxed} and $E_{\text{unrelaxed}}$ are the total energy for the relaxed and unrelaxed 2D-Xene nanoribbons, respectively, and n is the supercell size along x direction defined above. E_{edge} are calculated by including the SOC with in-plane antiparallel magnetization between two edges in the relaxed structures. In fact, only the relaxed silicene zigzag ribbons with 2a periodicity is spin polarized as previous reported [13,15,16]. All of the other relaxed structures are not spin polarized, in which the E_{edge} are calculated with only SOC. Comparing the edge energies with different periodicities in Table 2, structures with 3a periodicity have the lowest edge energies in 2D-Xene zigzag edges, which is consistent with the band filling of dangling bond states in Fig. 3. From Table 2, the relaxed structures with 2a and 4a periodicity are close in edge energy, while the edge energy difference between the 3a and 2a/4a structures increase from silicene to stanene. For comparison, the relaxed atomic and electronic band structures (nonmagnetic) with 2a and 3a periodicity are plotted in Fig. 4. With 2a periodicity, two degenerate states near the Fermi level give rise to a DOS peak at Fermi level, leading to an electronic instability. Only in the relaxed silicene-zigzag ribbons with 2a periodicity, two edges become spin polarized and are coupled antiparallel. The two bands near the Fermi level mainly come from the p_z orbitals of the edge atoms, while the p_y orbitals form bonding–antibonding states. For relaxed structures with 3a periodicity, a gap opens near Fermi level which further lowers the energy with respect to the structures with 2a periodicity. The ground states are insulating and non-magnetic.

In 1D atom chain, 1/3 filled band (2/3 unparied electron) would lead to a Peierls distortion in which three atoms come close and form trimer to open a gap [35]. However, we have 1D nanoribbon with finite ribbon width. As two edge atoms (A,B) come close (Fig. 4), the bonds between edge atoms and inner atoms would push the third edge atom (C) down. This is also happened on many crystal surface, such as Si (100) surface [36]. Fig. 5 shows the band structure and projected charge density of bonding and antibonding states in relaxed 9 × 3 germanene nanoribbons with one edge passivated by hydrogen atoms. The unpassivated edge atom A and B move towards each other and form bonding states with mainly p_y orbital character, while the antibonding states are formed on edge atom C. With structure reconstruction, the unpaired electron on edge atom C are transferred to edge atom A and B which forms bonding and antibonding states and opens a band gap. Only the edge states (Ge_H:p_z) of the passivated edge atom are left near the Fermi level.

5. Tight binding model

The phonon dispersion can be used to check the dynamic stability of the relaxed structures. However, the calculation of the phonon dispersion for relaxed structures with low symmetries are expensive in the present system. For example, the total number of supercells with different finite displacements can be as high as several hundred. In this paper, instead of calculating the phonon dispersion, we constructed a tight binding model based on the maximally localized Wannier functions (MLWFs) to better understand the 3a periodicity of edge reconstruction. For the fact that the bonding interaction has a mixing of sp^2 and sp^3 hybridization in the buckled 2D-Xenens, the Bloch wavefunctions are projected onto atom-centred sp^3 orbitals. For germanene monolayer, the 8 × 8 tight binding Hamiltonian is constructed with 4 sp^3-backward like orbitals that are maximally localized on each Ge atom in primitive cell shown in Fig. 6:

$$H(\boldsymbol{k}) = \begin{pmatrix} H_{AA}(\boldsymbol{k}) & H_{AB}(\boldsymbol{k}) \\ H_{BA}(\boldsymbol{k}) & H_{BB}(\boldsymbol{k}) \end{pmatrix} \tag{2}$$

The Bloch wave functions resulting from VASP calculation are transformed to an orthogonal set of Wannier functions by

$$|\psi_{\boldsymbol{k}\alpha}\rangle = \frac{1}{\sqrt{N}} \sum_{\boldsymbol{R}} e^{i\boldsymbol{k}\cdot(\boldsymbol{R}+\tau_\alpha)} |\boldsymbol{R}+\tau_\alpha\rangle \tag{3}$$

in which index α represents the A or B sublattice and $|\boldsymbol{R}+\tau_\alpha\rangle$ denotes the Wannier function for different orbitals at site $\boldsymbol{R}+\tau_\alpha$. In the tight binding Hamiltonian, the hopping parameters can be expressed in the form of Wannier function by

$$\begin{aligned} H_{\alpha\beta}(\boldsymbol{k}) &= \langle\psi_{\boldsymbol{k}\alpha}|H|\psi_{\boldsymbol{k}\beta}\rangle \\ &= \frac{1}{N} \sum_{\boldsymbol{R}\boldsymbol{R}'} e^{i\boldsymbol{k}\cdot(\boldsymbol{R}+\tau_\alpha-\boldsymbol{R}'-\tau_\beta)} \langle\boldsymbol{R}+\tau_\alpha|H|\boldsymbol{R}'+\tau_\beta\rangle \end{aligned} \tag{4}$$

in which $\langle\boldsymbol{R}+\tau_\alpha|H|\boldsymbol{R}'+\tau_\beta\rangle = t_{\alpha\beta}(\boldsymbol{R}-\boldsymbol{R}')$. The bandstructure for germanene monolayer based on Wannier function basis fit quite well with that from DFT calculations in the energy range we are interested at as shown in Fig. 6. Only nearest and next nearest hopping are included

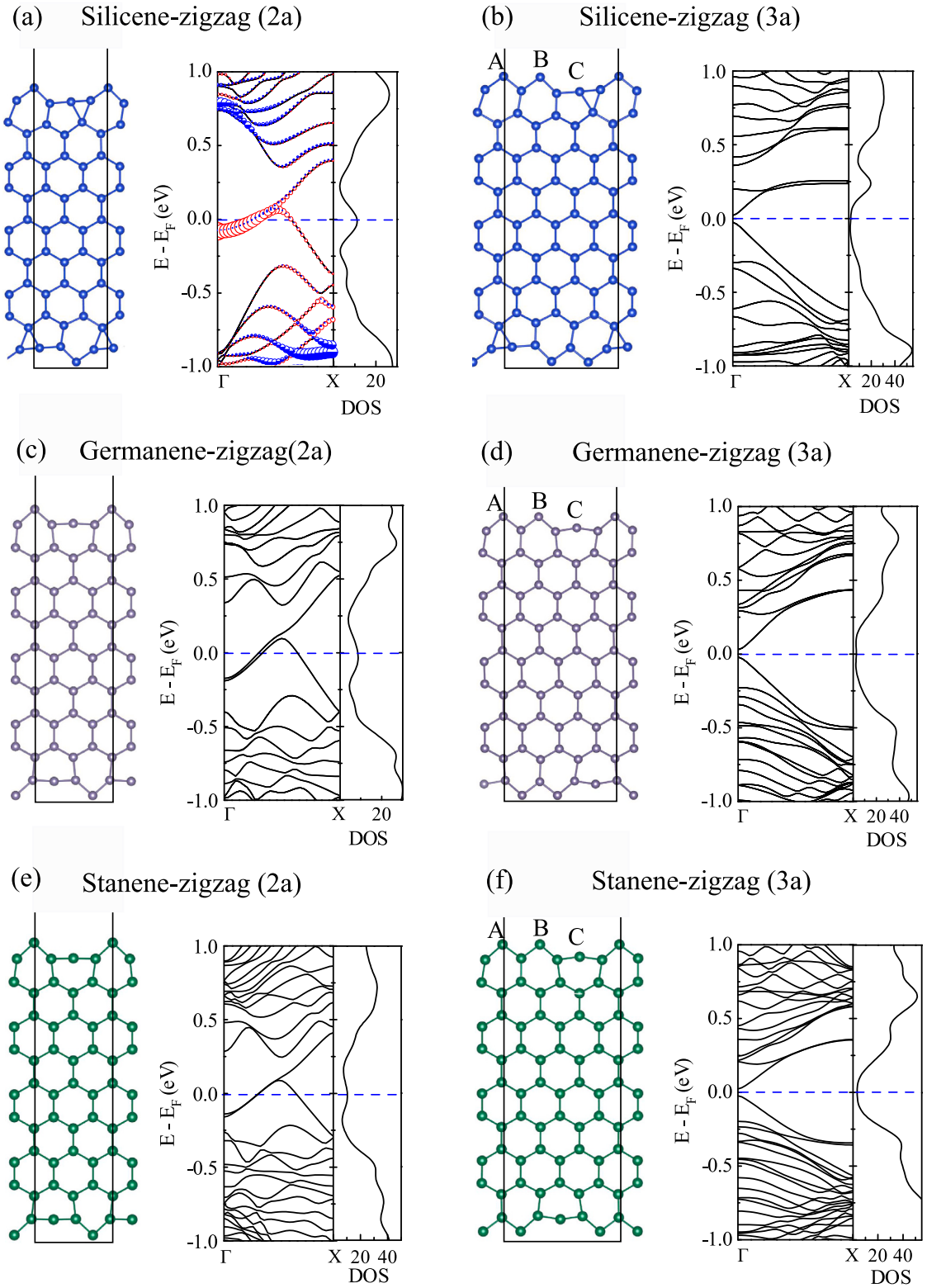

Fig. 4. Band structures (nonmagnetic) and atomic structures of relaxed zigzag ribbon with 2*a* and 3*a* periodicity for silicene (a, b), germanene (c, d), and stanene (e, f), respectively. A, B, C label the edge atoms in structures with 3*a* periodicity. The spin orbit coupling is included. The contribution from edge atoms p_z and p_y orbitals are show as open red circles and half-filled blue circles, respectively in (a, c, e) where the symbol size is proportional to the population of the corresponding state.

in the tight binding model. It should be noted that although the projected MLWFs are not most "physical" Wannier functions, this still can indicate the bonding interaction between Ge atoms qualitatively. The projected MLWFs on each Ge atom are shown in the rhs of Fig. 6. The first three Wannier functions are degenerate and mostly in-plane involved in the formation of σ bonds between Ge atoms, while the last one lies out of plane forming π bonds.

The hopping parameters for the nearest neighbours in the unit cell obtained from the Wannier projection are listed in Table 3. We can see that the buckling in germanene introduces the hopping between

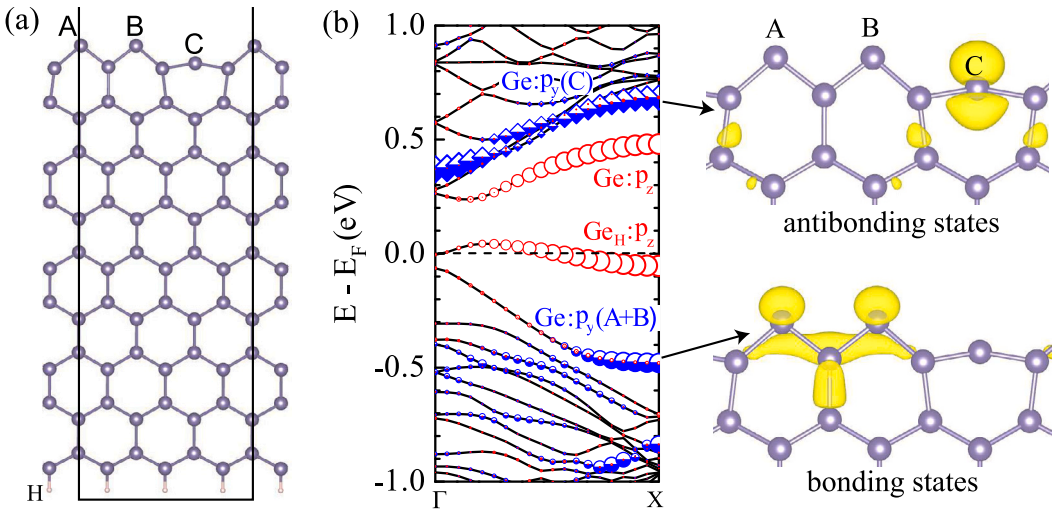

Fig. 5. (a) Atomic structure and (b) orbital projected band structure (without SOC and spin polarization) of relaxed germanene zigzag ribbon with hydrogen passivation on bottom edge. A, B, C label the edge atoms in structures with $3a$ periodicity. The band decomposed partial charge density for the edge bonding and antibonding orbitals are also shown in (b). The isosurface levels are 0.004 $e/\forall^3$. The contribution from edge atoms p_z and p_y orbitals are show as open red circles and half-filled blue circles, respectively in (b) where the symbol size is proportional to the population of the corresponding state.

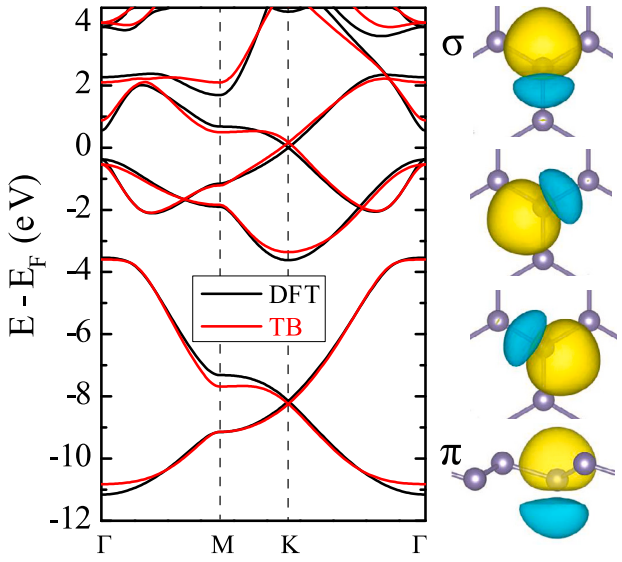

Fig. 6. Comparison of bands structures of germanene monolayer from DFT calculation and TB model based on Wannier function basis. Surface plot for the maximally localized sp^3-like Wannier functions. The yellow and blue regions indicate positive and negative values of the real part of the wave-function amplitudes. Considering the bonding interactions, the first three are labelled as σ orbitals and the last one is labelled as π orbital.

Table 3
Hopping integrals t (eV) and buckling δ (Å) of monolayer germanene, unrelaxed and relaxed 9 × 3 zigzag edge with three edge atoms (A, B, C). Only the nearest hopping parameters are shown in the table.

	ϵ_σ	ϵ_π	$t_{\sigma\sigma}$	$t_{\pi\pi}$	$t_{\sigma\pi}$	δ
germanene	−0.35	−1.15	−1.33	0.51	±1.43	0.69
unrelaxed	−2.59	−1.25	−1.89	0.19	±1.03	0.69
Ge A	−2.37	−1.47	−2.79	0.20	±0.56	0.46
Ge B	−2.22	−1.52	−2.61	0.35	±0.47	0.42
Ge C	−2.64	−1.74	−2.09	0.24	±0.88	0.58

in-plane and out-of-plane orbitals ($t_{\sigma\pi}$), indicating the hybridization between these orbitals. With respective to germanene, the decreased $t_{\pi\pi}$ at unrelaxed zigzag edge indicates a charge transfer from π orbitals to σ orbitals, which enhances the σ bonding interaction indicated by the enhanced hopping between σ orbitals ($t_{\sigma\sigma}$). This confirms the formation of extra σ bond between edge atoms and inner atoms as indicated in Fig. 3. After the edge reconstruction, two edge atoms (Ge 'A' and 'B') move together and one (Ge C) moves down to the inner part. The reduced buckling (δ) of the edge atoms results in a decrease of $t_{\sigma\pi}$ accompanied by an increase on both the $t_{\pi\pi}$ and $t_{\sigma\sigma}$. The relative large hopping between σ orbitals ($t_{\sigma\sigma}$) on edge atom 'A' and 'B' indicate an enhanced σ bonds (bonding states in Fig. 5(b)) between edge atoms and their nearest neighbours as indicated in Fig. 5(b), which formed by the unpaired 2/3 electron left on each edge atom in Fig. 3. The $t_{\sigma\sigma}$ of edge atom 'C' is much smaller than that on "A" and "B", indicating a charge transfer from edge atom 'C' to 'A' and 'B' and forms the antibonding orbitals in Fig. 5(b). As a result, this Peierls-like edge reconstruction opens a band gap near the Fermi level as seen in Fig. 4.

6. Discussion

For the applications in the nanodevices, the electronic states induced by the edge of 2D materials that affect the bulk properties cannot be ignored. In contract to the simple sp^2 hybridization between carbon bonds in graphene, the mixing of sp^2 and sp^3 hybridization in 2D-Xene gives rise to more challenges to identify these electronic states induced by the edges and their effects on the bulk electronic and structural properties. From the projected band structures shown in Fig. 3, we can find that the π edge states mainly consist of p_z orbitals, while the p_y orbitals contribute to the dangling bond states. It looks like a typical sp^2 hybridization where the bonding between atoms are dominated by the in-plane hybridized sp^2 orbitals. However, in 2D-Xene (X = Si, Ge, Sn) nanoribbons, due to the structural buckling, part of the dangling states (mainly sp^2 orbitals) hybrid with the edge states (mainly p_z orbital).

$$|\psi\rangle = sin\theta|\psi_{sp^2}\rangle + cos\theta|\psi_{p_z}\rangle. \quad (5)$$

This leads to the formation of extra bonding states with inner atoms by a charge transfer from edge states to dangling bond states at the unrelaxed zigzag edges (Fig. 3). As a result, 2/3 unpaired electron (mainly sp^2 orbitals) is left on the dangling bond states. After the structural relaxation, a Peierls-like distortion occurs with "3a" periodicity because of the "1/3" band filling of the dangling bond states. From silicene to stanene, the dispersion of dangling bond states in Fig. 3 is enhanced by the increased structural buckling and hybridization between sp^2 and p_z orbitals, which should change the band filling of the dangling bond states. However, for 2D-Xene (X = Si, Ge, Sn) zigzag nanoribbons, the

increased buckling is accompanied with an increase of lattice constant. The hopping between neighbouring orbitals do not change much from 2D silicene to stanene, which gives $3a$ periodicity for all 2D-Xene (X = Si, Ge, Sn) zigzag nanoribbons. It should be noted that the width of the nanoribbons in the calculations is large enough to minimize the interaction between two edges and mimic the edge of 2D Xene, while the very narrow nanoribbons could have different electronic and structural properties for the significant interactions between edges.

For the great potential applications in the silicon based semiconductor industry, edge reconstruction of the silicene zigzag nanoribbon have been intensively investigated [13,14,16,37]. A (2 × 1) reconstructed edge structure with a triangle-pentagon pair defect at the edges was reported for the zigzag Si nanoribbon. However, in order to reproduce the (2 × 1) reconstructed edges a tetragonal cell doubled along the ribbon direction is adopted in their calculations, where the edges would be reconstructed differently with longer tetragonal cell. The same reconstructed edges are found in our calculations (see Fig. 4(a)). As shown in Fig. 4(a), an extra bond is formed clearly between the edge and inner atoms. From the projected band structures, we can see that the bonding–antibonding bands mainly consist of p_y orbitals, while the p_z orbitals are left near the Fermi level. In the unrelaxed silicene zigzag ribbons, due to the structural buckling, a charge transfer from p_z orbitals to orbitals p_y push the p_z orbitals above the Fermi level as indicated in Fig. 3(b). In the relaxed structure with $2a$ periodicity, the p_y dangle bond states form extra bond with inner atoms, where only the p_z edge states are left near the Fermi level. The charge come back from the p_y orbital states to the p_z orbital states. Because of the reconstruction of the edges, the unbonded p_z edge states are not the same as the edge states in H-passivated edges where the dangling bond states are fully compensated by the hydrogen atoms. The unbonded p_z orbitals can lead to spin polarization with two edges coupled antiparallel. On the other hand, the structure can be further relaxed by a charge transfer from the unbonded p_z states to the p_y states, in which three edge atoms form bonding–antibonding states shown in Fig. 5(b), resulting in a relaxed structure with $3a$ periodicity.

The spin orbit coupling in 2D-Xene could play an important role on the edge electronic states. However, for the structural relaxation, the driving forces are mainly from the partially occupied dangling bond states, in which the SOC effect does not change the band filling of the dangling bond states. As discussed in Section 4, the affect of SOC on the forces are smaller than the force converge criterion (0.001 eV/Å). In fact, the SOC has a relative significant effect on the total energy (75 meV per edge atoms energy gain with respect to the NM states) but not the forces which is the gradient of potential energy with respect to displacement. Therefore, for simplicity, in our work the SOC is included only for the total energy calculations of relaxed structures but not the structural relaxation. Including SOC in the structural relaxation will not change the main results and conclusion in this work. The most stale structures have reconstructed edges with $3a$ periodicity and are non-magnetic with a small gap near the Fermi level.

The substrate material on which the 2D-Xene are grown can influence the buckling within the 2D layer, resulting from the Van der Waals interaction between them. Zhang et al. reported the germanene grown on the Ge_2Pt substrate have a lattice constant of 4.3 Å and a relative small buckling of 0.2 Å [1], corresponding to 6% tensile strain. However, they found a $4a$ periodicity at the zigzag edge of germanene. Our calculations are performed at zero Kelvin, while most of the experiment are done at room temperature. As indicated in Section 4, the edge energy difference between the relaxed structures with different periodicities are on the scale of a few tens meV. At room temperature, the thermal energy (~ 25 meV) might affect the periodicity of the zigzag edges. In addition, the edge band filling and the edge reconstruction can be changed by the possible charge transfer between the substrate and the material or tuned by external electric field.

7. Conclusion

In conclusion, we have investigated the zigzag edge reconstruction in 2D-Xene (X = Si, Ge, Sn) nanoribbons by performing first principles calculations and found ground-state edge reconstructions with $3a$ periodicity, which opens a band gap and shows non-magnetic ground states. The edge reconstruction is determined by the one-third band filling of the dangling bond states, which originates from the buckling of the atomic lattice. The buckling of the 2D-Xene edge atoms introduces the hopping between π and σ orbitals that reconfigures the band filling and bonding interaction at the edges. This work offers fundamental insights to the electronic and structural reconstructions at the pristine zigzag edges of 2D-Xene nanoribbons, which promotes the future applications related to 2D-Xene edge states and engineering.

Declaration of competing interest

The authors declare that they have no known competing financial interests or personal relationships that could have appeared to influence the work reported in this paper.

Data availability

Data will be made available on request.

Acknowledgements

This work was financially supported by the “Nederlandse Organisatie voor Wetenschappelijk Onderzoek” (NWO) through the research programme of the former “Stichting voor Fundamenteel Onderzoek der Materie”, (NWO-I, formerly FOM) and through the use of supercomputer facilities of NWO “Exacte Wetenschappen” (Physical Sciences). Y. Gao was additionally supported by the start-up grant of “Anhui Normal University, China”.

References

[1] L. Zhang, P. Bampoulis, A. van Houselt, H.J. Zandvliet, Two-dimensional Dirac signature of germanene, Appl. Phys. Lett. 107 (11) (2015) 111605, http://dx.doi.org/10.1063/1.4931102.
[2] A. Molle, J. Goldberger, M. Houssa, Y. Xu, S.-C. Zhang, D. Akinwande, Buckled two-dimensional xene sheets, Nature Mater. 16 (2) (2017) 163–169, http://dx.doi.org/10.1038/NMAT4802.
[3] P. Li, X. Li, W. Zhao, H. Chen, M.-X. Chen, Z.-X. Guo, J. Feng, X.-G. Gong, A.H. MacDonald, Topological Dirac states beyond π-orbitals for silicene on SiC (0001) surface, Nano Lett. 17 (10) (2017) 6195–6202, http://dx.doi.org/10.1021/acs.nanolett.7b02855.
[4] S. Rachel, M. Ezawa, Giant magnetoresistance and perfect spin filter in silicene, germanene, and stanene, Phys. Rev. B 89 (19) (2014) 195303, http://dx.doi.org/10.1103/PhysRevB.89.195303.
[5] C.-C. Liu, W. Feng, Y. Yao, Quantum spin hall effect in silicene and two-dimensional germanium, Phys. Rev. Lett. 107 (7) (2011) 076802, http://dx.doi.org/10.1103/PhysRevLett.107.076802.
[6] A. Acun, L. Zhang, P. Bampoulis, M. Farmanbar, A. van Houselt, A.N. Rudenko, M. Lingenfelder, G. Brocks, B. Poelsema, M.I. Katsnelson, H.J.W. Zandvliet, Germanene: the germanium analogue of graphene, J. Phys.: Condens. Matter 27 (2015) 443002, http://dx.doi.org/10.1088/0953-8984/27/44/443002.
[7] A. Nijamudheen, R. Bhattacharjee, S. Choudhury, A. Datta, Electronic and chemical properties of germanene: the crucial role of buckling, J. Phys. Chem. C 119 (7) (2015) 3802–3809, http://dx.doi.org/10.1021/jp511488m.
[8] M. Kurpas, P.E.F. Junior, M. Gmitra, J. Fabian, Spin-orbit coupling in elemental two-dimensional materials, Phys. Rev. B 100 (12) (2019) 125422, http://dx.doi.org/10.1103/PhysRevB.100.125422.
[9] J.L. Lado, N. García-Martínez, J. Fernández-Rossier, Edge states in graphene-like systems, Synth. Met. 210 (2015) 56–67, http://dx.doi.org/10.1016/j.synthmet.2015.06.026.
[10] Y.-L. Song, Y. Zhang, J.-M. Zhang, D.-B. Lu, Effects of the edge shape and the width on the structural and electronicproperties of silicene nanoribbons, Appl. Surf. Sci. 256 (2010) 6313–6317, http://dx.doi.org/10.1016/j.apsusc.2010.04.009.
[11] J. Kunstmann, C. Özdoğan, A. Quandt, H. Fehske, Stability of edge states and edge magnetism in graphene nanoribbons, Phys. Rev. B 83 (4) (2011) 045414, http://dx.doi.org/10.1103/PhysRevB.83.045414.

[12] J.N. Rodrigues, P.A.D. Gonçalves, N. Rodrigues, R. Ribeiro, J.L. Dos Santos, N. Peres, Zigzag graphene nanoribbon edge reconstruction with stone-Wales defects, Phys. Rev. B 84 (15) (2011) 155435, http://dx.doi.org/10.1103/PhysRevB.84.155435.

[13] C. Cahangirov, M. Topsakal, E. Akturk, H. Sahin, S. Ciraci, Two- and one-dimensional honeycomb structures of silicon and germanium, Phys. Rev. Lett. 102 (2009) 236804, http://dx.doi.org/10.1103/PhysRevLett.102.236804.

[14] M. Ferri, G. Fratesi, G. Onida, A. Debernardi, Optical properties of shortest-width zig-zag silicene nano-ribbons: Effects of local fields, Micro Nano Eng. 1 (2018) 37–41, http://dx.doi.org/10.1016/j.mne.2018.10.002.

[15] M. Ferri, G. Fratesi, G. Onida, A. Debernardi, Ab initio study of the structural, electronic, magnetic, and optical properties of silicene nanoribbons, Phys. Rev. B 99 (2019) 085414, http://dx.doi.org/10.1103/PhysRevB.99.085414.

[16] R. Li, J. Zhou, Y. Han, J. Dong, Y. Kawazoe, A new (2 × 1) reconstructed edge structure of zigzag Si nanoribbon: First principles study, J. Chem. Phys. 139 (2013) 104703, http://dx.doi.org/10.1063/1.4820943.

[17] J.C. Meyer, C. Kisielowski, R. Erni, M.D. Rossell, M.F. Crommie, A. Zettl, Direct imaging of lattice atoms and topological defects in graphene membranes, Nano Lett. 8 (11) (2008) 3582–3586, http://dx.doi.org/10.1021/nl801386m.

[18] K. He, A.W. Robertson, S. Lee, E. Yoon, G.-D. Lee, J.H. Warner, Extended klein edges in graphene, ACS Nano 8 (12) (2014) 12272–12279, http://dx.doi.org/10.1021/nn504471m.

[19] P. Sessi, J.R. Guest, M. Bode, N.P. Guisinger, Patterning graphene at the nanometer scale via hydrogen desorption, Nano Lett. 9 (12) (2009) 4343–4347, http://dx.doi.org/10.1021/nl902605t.

[20] Z. Liu, K. Suenaga, P.J. Harris, S. Iijima, Open and closed edges of graphene layers, Phys. Rev. Lett. 102 (1) (2009) 015501, http://dx.doi.org/10.1103/PhysRevLett.102.015501.

[21] J.N.B. Rodrigues, P.A.D. Goncalves, N.F.G. Rodrigues, R.M. Ribeiro, J.M.B.L. dos Santos, N.M.R. Peres, Zigzag graphene nanoribbon edge reconstruction with stone-Wales defects, Phys. Rev. B 84 (2011) 155435, http://dx.doi.org/10.1103/PhysRevB.84.155435.

[22] Y.-W. Son, M.L. Cohen, S.G. Louie, Half-metallic graphene nanoribbons, Nature 444 (2006) 347–349, http://dx.doi.org/10.1038/nature05180.

[23] Y.-W. Son, M.L. Cohen, S.G. Louie, Energy gaps in graphene nanoribbons, Phys. Rev. Lett. 97 (2006) 216803, http://dx.doi.org/10.1103/PhysRevLett.97.216803.

[24] A. Hattori, S. Tanaya, K. Yada, M. Araidai, M. Sato, Y. Hatsugai, K. Shiraishi, Y. Tanaka, Edge states of hydrogen terminated monolayer materials: silicene, germanene and stanene ribbons, J. Phys.: Condens. Matter 29 (2017) 115302, http://dx.doi.org/10.1088/1361-648X/aa57e0.

[25] B. van den Broek, M. Houssa, A. Lu1, G. Pourtois, V. Afanas'ev, A. Stesmans, Silicene nanoribbons on transition metal dichalcogenide substrates: Effects on electronic structure and ballistic transport, Nanoscale Res. 9 (11) (2016) 3394–3406, http://dx.doi.org/10.1007/s12274-016-1217-4.

[26] Y.-L. Songa, S. Zhang, D.-B. Lu, H. ru Xu, Z. Wang, Y. Zhang, Z.-W. Lu, Band-gap modulations of armchair silicene nanoribbons by transverse electric fields, Eur. Phys. J. B 86 (2013) 488, http://dx.doi.org/10.1140/epjb/e2013-31078-4.

[27] S. Rachel, M. Ezawa, Giant magnetoresistance and perfect spin filter in silicene, germanene, and stanene, Phys. Rev. B 89 (2014) 195303, http://dx.doi.org/10.1103/PhysRevB.89.195303.

[28] P.E. Blöchl, Projector augmented-wave method, Phys. Rev. B 50 (1994) 17953–17979, http://dx.doi.org/10.1103/PhysRevB.50.17953.

[29] G. Kresse, J. Hafner, *Ab* initio molecular dynamics for open-shell transition metals, Phys. Rev. B 48 (1993) 13115, http://dx.doi.org/10.1103/PhysRevB.48.13115.

[30] G. Kresse, J. Furthmüller, Efficient iterative schemes for *ab* initio total-energy calculations using a plane-wave basis set, Phys. Rev. B 54 (1996) 11169–11186, http://dx.doi.org/10.1103/PhysRevB.54.11169.

[31] G. Kresse, D. Joubert, From ultrasoft pseudopotentials to the projector augmented-wave method, Phys. Rev. B 59 (1999) 1758–1775, http://dx.doi.org/10.1103/PhysRevB.59.1758.

[32] J.P. Perdew, A. Zunger, Self-interaction correction to density-functional approximations for many-electron systems, Phys. Rev. B 23 (1981) 5048–5079, http://dx.doi.org/10.1103/PhysRevB.23.5048.

[33] A. Molle, J. Goldberger, M. Houssa, Y. Xu, S.-C. Zhang, D. Akinwande, Buckled two-dimensional Xene sheets, Nature Mater. 16 (2017) 163–169, http://dx.doi.org/10.1038/nmat4802.

[34] J.L. Lado, J. Fernández-Rossier, Magnetic edge anisotropy in graphenelike honeycomb crystals, Phys. Rev. Lett. 113 (2) (2014) 027203, http://dx.doi.org/10.1103/PhysRevLett.113.027203.

[35] J. Ahn, P. Kang, K. Ryang, H. Yeom, Coexistence of two different peierls distortions within an atomic scale wire: Si (553)-Au, Phys. Rev. Lett. 95 (19) (2005) 196402, http://dx.doi.org/10.1103/PhysRevLett.95.196402.

[36] A. Ramstad, G. Brocks, P.J. Kelly, Theoretical study of the Si(100) surface reconstruction, Phys. Rev. B 51 (1995) 14504, http://dx.doi.org/10.1103/PhysRevB.51.14504.

[37] M. Ferri, G. Fratesi, G. Onida, A. Debernardi1, Ab initio study of the structural, electronic, magnetic, and optical properties of silicene nanoribbons, Phys. Rev. B 99 (2019) 085414, http://dx.doi.org/10.1103/PhysRevB.99.085414.